The C-terminal domain of piggyBac transposase is not required for DNA transposition

Laura Helou, Linda Beauclair, Hugues Dardente, Peter Arensburger, Nicolas Buisine, Yan Jaszczyszyn, Florian Guillou, Thierry Lecomte, Alex Kentsis, Yves Bigot

The C-terminal domain of *piggyBac* transposase is not required for DNA transposition

Laura Helou[1], Linda Beauclair[1], Hugues Dardente[1], Peter Arensburger[2], Nicolas Buisine[3], Yan Jaszczyszyn[4], Florian Guillou[1], Thierry Lecomte[5], Alex Kentsis[6,7,8] and Yves Bigot[1,*]

[1] PRC, UMR INRAE 0085, CNRS 7247, Centre INRAE Val de Loire, 37380 Nouzilly, France

[2] Biological Sciences Department, California State Polytechnic University, Pomona, CA 91768, United States of America

[3] UMR CNRS 7221, Muséum National d'Histoire Naturelle, 75005 Paris, France

[4] Université Paris-Saclay, CEA, CNRS, Institute for Integrative Biology of the Cell (I2BC), 91198, Gif-sur-Yvette, France

[5] EA GICC 7501, CHRU de Tours, 37044 Tours Cedex 09, France

[6] Molecular Pharmacology Program, Sloan Kettering Institute, Memorial Sloan Kettering Cancer Center, New York, New York, USA

[7] Weill Cornell Medical College, Cornell University, New York, New York, USA

[8] Department of Pediatrics, Memorial Sloan Kettering Cancer Center, New York, New York, USA

[*]Corresponding author address: PRC, UMR INRA 0085, CNRS 7247, 37380 Nouzilly, France. Tel: +33 2 47 42 75 66, e-mail: yves.bigot@inrae.fr

Highlights

- The C-terminal CRD in *pble* transposases is not essential for transposition
- Two CRD-deficient *pble* transposases trigger transposition of *Ifp2*
- Proper and improper insertions occur when CRD-deficient transposases mediate mobility
- CRD-deficient and full-length *pble* transposases do not insert transposons at random
- Features of the domesticated transposase PGBD5 originate from wild type transposase

Abstract

PiggyBac(PB)-like elements (*pble*) are members of a eukaryotic DNA transposon family. This family is of interest to evolutionary genomics because *pble* transposases have been domesticated at least 9 times in vertebrates. The amino acid sequence of *pble* transposases can be split into three regions: an acidic N-terminal domain (~100 aa), a central domain (~400 aa) containing a DD[D/E] catalytic triad, and a cysteine-rich domain (CRD; ~90 aa). Two recent reports suggested that a functional CRD is required for *pble* transposase activity. Here we found that two CRD-deficient *pble* transposases, a PB variant and an isoform encoded by the domesticated PB-derived vertebrate transposase gene 5 (*pgbd5*) trigger transposition of the *Ifp2 pble*. When overexpressed in HeLa cells, these CRD-deficient transposases can insert *Ifp2* elements with proper and improper transposon ends, associated with deleterious effects on cells. Finally, we found that mouse CRD-deficient transposase *Pgbd5*, as well as PB, do not insert pbles at random into chromosomes. Transposition events occurred more often in genic regions, in the neighbourhood of the transcription start sites and were often found in genes predominantly expressed in the human central nervous system.

Keywords: transposon / DNA cleavage / neuron / insertion preference / vertebrate

Abbreviations:

CRD: cysteine-rich domain

gDNA: genomic DNA

GFP: green fluorescent protein

ISCR: insertion sites-containing regions

NeoR : neomycin resistance

NLS: nuclear localisation signal

ORF: open reading frame

PB: *piggyBac* transposase

pble: *piggyBac*-like element

PGBD or *pgbd*: "*piggyBac* derived transposase" protein or gene

STIR: sub-terminal inverted repeats

SV40: simian virus 40

TE: transposable element

TIR: terminal inverted repeats

TSD: target site duplication

Introduction

Transposable elements (TEs) gather diverse discrete DNA sequences of prokaryotic and eukaryotic origins that use a wide range of mobility mechanisms to transpose within the genome of their hosts [1-4]. *PiggyBac-like* elements (*pble*) consist of a family of DNA transposons that have so far only been found in animal genomes and with copy numbers that vary widely between host species [5]. *Pbles* are able to jump from one chromosomal locus to another using cut-and-paste transposition which is enzymatically catalysed by the transposase they encode. The first *pble* to be identified was *Ifp2* (a.k.a. *piggyBac*) from the cabbage looper moth *Trichoplusia ni* (Lepidoptera) [6]. It is the reference element in the *piggyBac* family for academic research purposes [7]. The *Ifp2* DNA sequence is 2476 bp in length and contains an open reading frame (ORF) coding a 594 amino acid transposase named PB. The *Ifp2* DNA sequence is flanked by 13 bp long terminal inverted repeats (TIR) and by 19 bp long subterminal inverted repeats (STIR) located internally at 3 and 31 nucleotides of distance of 5' and 3' TIR inner ends, respectively. PB excises the transposon from its donor chromosomal locus and reinserts it into a TTAA motif, which gets duplicated upon insertion. Sequence analyses revealed that PB contains at least 3 domains. The first domain spans from residues 1 to 116, shows no overt structural features and displays an acidic pI of 4.41. The second domain is a macro domain that extends from residues 117 to 535 and has a basic pI (9.29); it contains several highly conserved residues, including the predicted catalytic residues (D268, D346 and D447) that are required for all transposition steps. On both sides of the catalytic domain (residues 263 to 457), recent structures obtained by cryo-electron-microscopy [8] revealed two DNA binding sub-domains (residues 117 to 263 and 457 to 535, respectively) that bind to *Ifp2* TIRs. Finally, the third domain spans from residues 559 to 594, and contains a cysteine-rich domain (CRD, pI=9.07) for which the atomic structure was first solved by nuclear magnetic resonance [9]. This CRD was shown to bind to a 5'-TGCGT-3'/3'-ACGCA-5' motif that is contained within the 19 bp subterminal inverted repeat between positions 178 and 199 of the *Ifp2* sequence [9]. The CRD was also found to be vital for the dimerization of PB [10], the removal of the last seven residues being sufficient to yield a monomeric protein that still binds to *Ifp2* ends *in vitro*. Finally, this CRD contains a nuclear localisation signal (NLS) that is required to mediate PB nuclear localisation [11].

Two studies [9,10] proposed non-exclusive roles for the CRD and the ability of PB to mediate transposition. In the first study, the authors concluded that the CRD was essential for *Ifp2* transposition because the use of a CRD-deficient PB (PB.1-558) in an integration assay performed in mammalian cells did not lead to an increase in integration activity compared to controls done in the absence of the transposase [9]. The second study proposed that PB dimerisation might serve to prevent excessive transposition of *Ifp2* since removal of the CRD led the monomeric PB to be more active in transposition excision [10]. It is also possible that the absence of the CRD may cause

cytosolic retention since it contains a nuclear localization sequence (NLS).

Here we aimed to determine whether PB.1-558 fused to a simian virus 40 (SV40) NLS was able to mediate the transposition of *Ifp2* into human cell chromosomes. First, we showed that both PB.1-558 and PB.NLS-1-558 had a negative effect on obtaining clones in integration assays. Second, we found that PB.NLS-1-558 was able to carry out the transposition of *Ifp2* elements. Third, we compared the properties of PB.NLS-1-558 with those of another CRD-deficient *piggyBac* protein, the domesticated murine and human PGBD5 protein. Fourth, we evaluated the quality of *Ifp2* ends neo-integrated into chromosomes by PB and the two CRD-deficient proteins, PB.NLS-1-558 and PGBD5. Finally, we determined whether the three proteins used similar or different pools of chromosomal insertion sites, whatever the state of *Ifp2* transposon ends.

Results

PB.1-558 needs an NLS to locate into nuclei.

We made a CRD-deficient PB mutant (PB.1-558) and a construct in which its N-terminal end was fused with a SV40 NLS (PB.NLS-1-558). Such a position for the NLS does not modify the transposition activity of PB and preserves the activity of the added localization motif or protein domain [12,13]. To assess cellular localization of both proteins we made two more constructs in which the green fluorescent protein (GFP) was C-terminally fused to PB.1-558 and PB.NLS-1-558. An expression vector encoding GFP was used as a diffusion control within the cytoplasm and nucleus (Fig. 1a-c) and a vector encoding a PB-GFP fusion was used as a control for active import into the nuclei (Fig. 1d-f) [11]. Our data revealed that PB.1-558 is not enriched in the nucleus (Fig. 1g-i), which contrasts with its PB.NLS-1-558 counterpart that is almost completely nuclear (Fig. 1j-l).

PB variants display cytotoxicity

Prior to assaying the ability of the full-length PB, PB.1-558, and PB.NLS-1-558 to trigger transposition of an *Ifp2* source, we checked whether these proteins impacted random integration rates into HeLa cell chromosomes. We used a DNA plasmid containing a gene cassette coding for a neomycin resistance (NeoR) without the *Ifp2* sequence, the pBSK-NeoR plasmid. This was performed using a classic integration assay (see material and methods section). We observed that the integration rate of pBSK-NeoR into chromosomes was significantly lower in the presence of each of the three variants compared to a control GFP sequence (Fig. 2a; ~1.25, 1.31, 2.67 folds (1/fold change) for PB, PB.1-558, and PB.NLS-1-558, respectively). This indicated that PB and its variants have a deleterious effect on cells, including those that display random and stable integrations of NeoR into their chromosomes. The cytotoxicity of PB.NLS-1-558 is higher than that

of PB and PB.1-558.

The results of integration assays (Fig. 2b) performed with the *Ifp2*-NeoR transposon donor plasmid confirmed that PB.1-558 has a negative effect on obtaining NeoR clones. The number of clones was 1.5 times lower than that obtained with the GFP control and 60 times lower than that obtained with PB. This indicated that integration assays performed with PB.1-558 are affected by both: 1) the cytotoxicity of PB.1-558, and 2) the integration of the NeoR cassette into chromosomes.

The number of NeoR clones obtained with PB.NLS-1-558 was 2.5 times higher than that with the GFP control. Due to the cytotoxicity of PB.NLS-1-558, this number was likely underestimated. After correcting for PB.1-558 toxicity rate (Fig. 2c) we estimate the number of integration events to be ~7 times higher what is found with the GFP control. Overall, this means that PB.NLS-1-558 is roughly 8 times less efficient than PB for obtaining NeoR clones in an integration assay done in HeLa cells. Because cytotoxicity hampered our ability to directly evaluate integration rates and was likely dose-dependent as observed with PGBD5 [14], we focused our investigation on the ability of PB.NLS-1-558 to trigger *Ifp2* transposition by characterizing integration events into chromosomes by NeoR clones.

Features of sites targeted by PB and PB.NLS-1-558 when integrating *Ifp2* into chromosomes

To verify the presence of transposition events and to determine their sequence features, we produced fragment populations corresponding to *Ifp2*-chromosome junctions. These were made by LAM-PCR using genomic DNA (gDNA) of NeoR clone populations that were sequenced using Illumina Miseq technology. To prepare gDNA samples we used ~60000 clones from integration assays done with *Ifp2*-NeoR and PB, and ~1000 clones from integration assays done with *Ifp2*-NeoR and PB.NLS-1-558. Previous results of integration assays performed in HEK293 cells found that the rate of *Ifp2* integration into chromosomes by proper transposition (i.e. with a perfect duplication of the "TTAA" TSD and conservation of the TIR sequence) was about 96-98% when PB was used as a transposase source [15,16].

Using DNA sequence alignments, we characterized 7623 *Ifp2*/chromosome junctions resulting from integration events mediated by PB and 516 junctions mediated by PB.NLS-1-558, with *Ifp2*-NeoR as a transposon source (supplementary Table 1a and 2a). Sequenced junctions at the 5' and the 3' of *Ifp2* ends were not equally represented in the sequence data, likely because of efficiency differences at certain steps of DNA fragment amplification during the LAM-PCR. Sequence junctions were further examined taking into account the conservation of TSD and TIR sequences, two features that were required to keep the capacity of neo-inserted elements to be efficiently remobilized during excision and insertion, i.e. to remain "active in transposition" [15,16]. Four kinds of junctions were observed: those displaying i) a full TIR sequence and a TTAA TSD (red

bars from positions 101 to 104 and 2222 to 2225 in Fig. 3), ii) a region containing an intact TIR and a TTAA TSD juxtaposed to a little piece of plasmid backbone (black bars from positions 1 to 100 and 2226 to 2301 in Fig. 3a and b), iii) no TTAA TSD but a full TIR sequence (blue bars from positions 102 to 105 and 2218 to 2221 in Fig. 3), and iv) no TIR sequence lacking one or several nucleotides at its outer end (black bars from positions 107 to 178 and 2147 to 2217 in Fig. 3). The summary of results in Table 1 indicates that the rate of proper events when PB was used as a transposase was similar to that previously observed in other cell types, but 3.3% of junctions nevertheless displayed improper TSD, TIRs or both. Interestingly, 19.0% of junctions mediated by PB.NLS-1-558 were found to be proper, thus demonstrating that this variant is able to trigger canonical transposition events even though less efficiently than PB. Our results also indicated that PB.NLS-1-558 integrated *Ifp2* into non-canonical TSDs approximately 25 times more often than PB. Furthermore, TIRs were damaged or accompanied by a piece of backbone sequence of variable length juxtaposing the transposon in the transposon donor plasmid in about 65% of *Ifp2*/chromosome junctions (while they represented only 2.25% of junctions among integration events triggered by PB). These observations suggested that the observed junctions resulted from both proper transposition events and improper integration events that could be mediated by both PB variants, but the rates of each kind of integration events were dramatically different between the two proteins.

Next, we identified 5' and 3' junctions for events that occurred exactly at the same chromosomal insertion sites in both datasets. We observed that 7446 chromosomal sites were used and found 177 unambiguous insertion sites in our Lumpy raw file that were occupied several times. In these 177 sites, integration events occurred in both *Ifp2* orientations when mobility was mediated by PB (supplementary Table 1b). A careful examination of the resulting bam file with IGV [17] revealed 11 cases of putative single integration events (supplementary Table 1b, case highlighted in cyan blue). Among them, three corresponded to *Ifp2* transposons displaying at least one TIR damaged at its outer end, and one TIR was inserted into a duplicated TSD corresponding to a duplicated CATG motif. As previously described [18,19] we also found four sites in which both integration events occurred into non-canonical TSD (CATG, TATC, ACAT, TTCC; supplementary Table 1b) and 16 sites where two events occurred with the insertion of transposons with at least one improper end. These results suggest that virtually any type of non-canonical integration can be found at a very low frequency when *Ifp2* was transposed by PB. In data resulting from the transposition of *Ifp2* by PB.NLS-1-558, we found that 516 chromosomal sites were used and identified 32 unambiguous insertion sites for which integration events occurred in both orientations of the transposon. Four of these putatively corresponded to single integration events (supplementary Table 2b, case highlighted in cyan blue, two would correspond to canonical integrations by transposition and two

with non-canonical TIR or TSD). The main difference with PB is that improper events were dramatically more frequent when transposition was mediated by PB.NLS-1-558.

PGBD5 a natural domesticated CRD-deficient *pble* transposase

We compared the transposition features of the PB.NLS-1-558 variant to those of murine and human orthologues of the oldest domesticated *piggyBac* transposase since the origin of vertebrates, PGBD5 (Mm523 and Hs524) [20]. Alignment of three protein sequences (Fig. 4) revealed that both CRD-deficient proteins displayed an acidic N-terminal domain and a second domain with a basic pI (~9.2) containing an apparent catalytic triad composed of 3 acidic amino acid residues that were essential for transposition activity [20]. Another shared feature was their ability to trigger *Ifp2* transposition [14,21]. This transposition ability was rather unexpected for PGBD5 compared to PB.NLS-1-558 because the PGDB5 catalytic triad was not located at the same positions as in *pble* transposases (Fig. 3, bold residues highlighted in yellow). PGBD5 acquired a new putative NLS that is centrally located in the sequences of Mm523 and Hs524 (Fig. 3, RKRKKRK motif typed in green and underlined). In agreement with the literature [14] we observed that the ectopic expression of murine PGBD5 isoform of 523 amino acids (Mm523) reduced the apparent efficiency of obtaining NeoR clones (Fig. 5a) that is close to that of PB.NLS-1-558 in HeLa cells (Fig. 2a). In integration assays done with the *Ifp2*-NeoR transposon donor plasmid under experimental conditions similar to those used above for PB.NLS-1-558, the rate of NeoR clones obtained with Mm523 (Fig. 5b) was similar to that obtained with the GFP control. In order to verify whether this was due to PGBD5 cytotoxicity, we used a second cellular system developed in human rhabdoid tumor G401 cells and in which the endogenous expression of PGBD5 (Hs524) was found to have little impact on cell viability [14]. Under these experimental conditions, we found that the rate of NeoR clones was sevenfold higher than that of the GFP control (Fig. 5b). Together, this indicates that the expression rate of CRD-deficient *pble* transposases strongly impact the outcome of integration assays.

The sequence features of integration events were studied through *Ifp2*-chromosome junctions obtained with Mm523 and Hs524. We prepared gDNA samples from ~1800 and 1600 NeoR clones obtained from integration assays done with *Ifp2*-NeoR and, Mm523 or Hs524, respectively. Using the Mm523 gDNA sample, we obtained 1461 transposon/chromosome junctions that were analyzed as described above (supplementary Table 3a). The profiles of transposon/chromosome junctions were found to be similar between integration events mediated by PB.NLS-1-558 and Mm523 (Fig. 3c, and Table 2 versus last raw in Table1). This was also verified by examining chromosomal sites where we found integration events in both orientations within the 1461 chromosomal sites used (supplementary Table 3a and b). When the junctions were categorized and analyzed in terms of percentages at each *Ifp2* end for PB, PB.NLS-1-558 and Mm523 we observed that: i) proper

junctions occurred more often at the 3' end than at the 5'end (Fig. 6, red bars), and ii) among improper junctions, those without a canonical TSD and those located within TIR and juxtaposed with transposon sequences (Fig. 6, blue bars and internal black bars, i.e. wounds at transposition ends as exemplified in [22]) occurred more often than those located within the plasmid backbone sequences juxtaposed near the TSD and TIR of the donor plasmid (Fig. 3, flanking black bars). Using the Hs524 gDNA sample, we obtained 1051 transposon/chromosome junctions (supplementary Table 4a). The junction profile was overall similar to those of both CRD-deficient proteins (Fig. 3c and 6d), but it displayed a marked difference in that there were fourfold and twofold less proper insertion events by transposition than in those obtained with PB.NLS-1-558 and Mm523, respectively. Unexpectedly, this suggests that PGBD5 is more prone to trigger improper integration in rhabdoid tumor G401 cells, consistent with the proposal that PGBD5 exhibits aberrant activities in human rhabdoid tumors [14]. Since we observed that PB.NLS-1-558, Mm523 and Hs524 display similar junction profile, we wondered if their insertion site preferences might be similar.

Features of insertion sites targeted by PB variants and PGBD5 when integrating *Ifp2* into chromosomes

PB and PGBD5 have been shown to integrate *Ifp2* into intragenic regions more frequently than expected by chance, specifically within transcription start site (TSS) regions flanking (± 5 kbp) protein-coding genes [23-26]. Using our junction data, we observed that PB, PB.NLS-1-558, Mm523, Hs524 did not distributed *Ifp2* integrations at random into intergenic and intragenic regions (Fig. 7a; Chi2, $p = 2.08x10^{-95}$, $2.21x10^{-10}$, 0.0026, and $3.72x10^{-81}$ respectively), but with a significant enrichment for intragenic regions (hypergeometric test, $p << 0.01$ for the four proteins). Similar investigations were also done within regions flanking TSSs of five types of genes coding for: i) proteins, ii) non-coding RNA (ncRNA), iii) micro RNA (miRNA), or being annotated in hg38 as iv) pseudogenes or v) uncharacterized genes. We also found that *Ifp2* was integrated more frequently than expected by chance within regions flanking TSSs in the 5 types of genes, except for the two CRD-deficient proteins into uncharacterized genes (Fig. 7b; Chi2, $p = 2.58x10^{-9}$, $2.16x10^{-8}$, $8.27x10^{-12}$, and $3.43\ x10^{-9}$ respectively), and with a significant enrichment in each type of genes (hypergeometric test, $p << 0.01$ for the four proteins), except for the miRNA and ncRNA genes in the PB.NLS-1-558 and Mm523 datasets, respectively (hypergeometric test, $p = 0.043$ and 0.051). In addition to these global distribution features, a striking feature was that our Lumpy raw files, after manual investigation using IGV, contained 166 (i. e. 177-11), 24 (44-20), 23 (26-3) and 11 (13-2) chromosomal sites, each displaying a fragment containing the *Ifp2* element inserted in both orientations, i.e. inserted at least twice into these sites when integration events were mediated by PB, PB.NLS-1-558, Mm523 and Hs524, respectively. We also found common insertions sites

among the PB, PB.NLS-1-558, Mm523 and Hs524 datasets (Table 3, lines 1, 3 and 5). These insertion events occurred at the same nucleotide position site but this was not due to sample contamination since they resulted from *Ifp2* integration events in different orientations and in some cases from properly and improperly integrated *Ifp2* transposons. The number of these observations was increased when using a 1000 bp window on both sides at each chromosomal insertion site (Table 3, lines 2, 4 and 6; regions called below insertion sites-containing regions (ISCR)).

The choice of an insertion site by any *pble* transposase does not fully occur at random since a TTAA motif is used. In the human genome model hg38, there are 18,713,270 TTAA motifs. Public data about DNAse I hypersensitivity mapping revealed that 98% of them are located in open chromatin in HeLa cells (but also in HEK cells), i.e. accessible to DNA binding proteins such as transposases. This means that the probability of integrating an *Ifp2* transposon twice into a single target site lies about 1.8 $x10^{-7}$ in hg38. Taking into account the size of datasets used herein, to find several insertions by chance into the same site is therefore unexpected under our experimental conditions.

Given the putative impact of some specific genomic features of HeLa cells such as their aneuploidy [27-30], we further investigated ISCR features in other cell lines taking advantage of public datasets. We used three of them that were produced from integration assays performed with *Ifp2* and PB in HEK293 [23], in HCT116 [15] and in CD4+ [26] cells (21,967, 172,866 and 8954 chromosomal sites, respectively (Table S4a, b, c)).

First, we confirmed that the rate of insertions mediated by PB into intragenic regions in each of the four cell lines (HeLa, HEK293, HCT116 and CD4+; Table 4a, column 4) is 7 to 18% higher than expected by chance (51.6%; Table 4b, column 1). This preference could not be explained by the numbers of TTAA motifs in intragenic regions (53.1%; Table 3c, column 2), which is close to that expected by chance. In spite of variations of aneuploidy and chromatin profiles between the four cell lines, the insertion preference into intragenic regions does not appear to correlate to these features.

In order to verify the statistical consistency of insertion sites shared between datasets, all pairs of datasets were compared taking into account the variation of TTAA motif distribution between intra and intergenic regions (Table 4c). P-values indicated that the number of commonly used chromosomal insertion sites was significantly more elevated than expected by chance (Table 3; raws 1 to 16) whatever the window used around the insertion sites (0 or 1000 bp). We also observed that 18 ISCR were shared by the four datasets obtained with *Ifp2* and PB in the four cell lines.

We also examined insertion datasets obtained with the transposon *sleeping beauty* in HEK293 and CD4+ cells (28490 and 8290 insertion sites, respectively [15,26]). Taking into account the distribution of its TA targets in hg38 (Table 4c), results in Table 3 revealed that this transposon does not display a significant preference between available putative TA target sites. It displayed higher

rates of insertion into intragenic regions (~62.5%, Table 4a) than predicted by chance (51.6%, Table 4b). In contrast to PB, this can however be correlated with TA density that is dramatically increased in these regions (60.4%, Table 4c) compared to intergenic ones.

In all, our data reveal that PB, PB.1-558, Mm523 and Hs524 insert *Ifp2* preferentially into intragenic regions with some level of site preference between available TTAA target sites.

Features of genes targeted by *Ifp2* insertions mediated by PB variants and PGBD5

We wondered whether insertion site preferences of *pble* transposases might also be seen at the level of some intragenic regions. We postulated that experimental conditions of transposition assays are conducive to forced integration of transposons into chromosomes. Therefore, we predicted that insertions should be enriched among ISCR shared by several datasets than among those unique to each dataset.

In the ontology analysis done with the 410 genes overlapped by ISCR and shared by at least two datasets among those obtained with PB, PB.NLS-1-558, Mm523 and Hs524 in HeLa cells (Figure 6a), we found that 35/50 significant terms were directly related to the nervous system (Table 5). This issue was therefore further investigated by verifying whether there was an enrichment of "neuron genes" among ISCR overlapping with genes. For this purpose, we used the 6854 "neuron genes" identified in hg19 based on the expression properties of 29165 genes (protein-, ncRNA- and miRNA-coding plus some uncharacterized genes and pseudogenes) in 216 distinct human brain structures [31]. We found that neuronally expressed genes were significantly enriched in each of the PB, PB.NLS-1-558, Mm523 and Hs524 datasets obtained in HeLa cells (Table 4a, columns 5,6,7). They were again enriched among the 697 genes overlapped by ISCR that were shared by at least two of four datasets. This enrichment in neuron genes was 31.7-38.8% in each of the four datasets and 37.2% (259/697) among the 697 shared genes. These results therefore support the notion that neuron genes are preferred regions for *pble* transposases to insert *Ifp2*.

These observations were confirmed using datasets obtained in HEK293, HCT116 and CD4+ cells. First, we found that neuronally expressed genes were significantly enriched in each of the four datasets (Table 4a, columns 5,6,7). This did not appear to be related to the target density since the percentage of ISCR in those genes was found to be 3 to 8% more elevated than the rate of TTAA motifs in those genes (Table 4a, column 4 versus Table 4c, column 3). We found that genes overlapped by ISCR and shared by at least two of four datasets did not display a significant enrichment in neuron genes (3884/12618; 30.8%; Figure 6b). However, a very strong enrichment was found when only ISCR shared by the four datasets were kept for the analysis (705/1100, 64% neuron genes) and a strong depletion in neuron genes was found among genes occurring in only one dataset (2273/12186; 18.7%).

Finally, we evaluated whether the insertion preferences into neuronally expressed genes were specific to PB by analysing the same features in datasets obtained with two unrelated transposons [15,26]. Data obtained with *sleeping beauty* in HCT116 and CD4 cells and with a *TcBuster* in HCT116 cells indicated that both transposons also inserted more frequently into neuronally expressed genes than in other genes (Table 4a, column 4,5,6). Their insertion preferences were also about 6-8% above the density in their respective target motif (Table 4c, column 3). For *sleeping beauty*, we also found that there was an enrichment in neuronally expressed genes among genes that overlapped by ISCR and shared by both datasets (1143 neuron genes for 2813 genes; 40.63%) and a depletion in those which were only found in one dataset (2625/9791; 26.8%).

Altogether, these last results reveal that *pble* transposases insert *Ifp2* more often than expected by chance into neuronally expressed genes. However, this apparent preference is also displayed by *sleeping beauty* and very likely by *TcBuster*, indicating that it is not specific of *pble* transposases. This is not related to the gene size and the number of TTAA and TA because the densities in target motifs are very close in neuron and non-neuron genes (TTAA: 5.318 ± 0.029 and 5.114 ± 0.015 motifs/kbp, respectively; TA: 44.68 ± 0.156 and 44.07 ± 0.083 motifs/kbp, respectively). Therefore, this might result from the enhanced accessibility of neuronally expressed genes or their association with DNA repair and chromatin remodeling factors that support DNA transposition, a property that would be shared by multiple cell lines as exemplified here.

Discussion

This study generated two sets of novel insights. First, the two CRD-deficient transposases PB.NLS-1-558 and PGBD5 (Mm523 and Hs524) mediate canonical *Ifp2* transposition, but also non-canonical events that may result from events of improper transposition, transposase-dependent integration by recombination and random integration. We assume that these CRD-deficient transposases operate at a reduced efficiency than the "wild-type" or "full-length" *piggyBac* transposase but their cytotoxicity on host cells and the possibility that they do integration by transposase-dependent recombination indicated that they have nuclease activity, as previously suggested for PGBD5 isoforms [13]. Furthermore, cytotoxicity issues often arise from the balance between the level of expressed protein and the efficiency of mechanisms responsible for the maintenance of genome integrity, which varies widely from one cell line to another. Such effects could also be related to the cell cycle. This might explain why PB.NLS-1-558, which was always located in the nucleus, had a more negative effect than PB.1-558 (Fig. 2a), which was mainly cytoplasmic during most of the cell cycle and in contact with chromosomes only during the cell division phase.

The second insight from this work concerns the ability of PB and both CRD-deficient *pble*

transposases to trigger integration events that did not seem to occur at random into chromosomes. However, we cannot assume strict insertion site specificity of *pble* transposases since only a small part of the observed insertions events in datasets are the same, down to the same nucleotide position. However, our data demonstrated that these transposases displayed real preferences for insertion into regions containing genes and frequently close to their TSS. In addition, our results supported that *pble* transposases frequently targeted their *pble* insertions into genes committed to the central nervous system function. This last point will need further experimental confirmation. Indeed, the lengths of genes involved in nervous system function were, on average, longer than those of other genes (for review see [32]). An alternative interpretation might be that the insertion sites we found were preferentially located in neuronally expressed genes due to their size. However, our results take into account the genome coverage and the density in TTAA motif and support that the observed insertion preferences are not related these factors.

Contribution to the understanding of *piggyBac* transposition.

Previous studies suggested two roles for the CRD of PB. The CRD might be an essential component of DNA-binding to the ends of *Ifp2*, mandatory for transposition [9]. This was confirmed in another study, which also indicated that the CRD was essential for the assembly of the transposase dimer, the active oligomer form for transposition [10]. Here we demonstrate that two CRD-deficient *piggyBac* transposases were able to trigger proper *pble* transposition. Therefore, the CRD is not essential for transposition but seems necessary for triggering proper transposition events, probably by driving precise DNA cleavages at *pble* ends and directing a strict choice of TSD.

Evolutionary reasons for domesticating a CRD-deficient *pble* transposase

These results, as well as previously published data [14,20,21], have highlighted two properties of PB, and perhaps of other *pble* transposases, that may have previously been underestimated in the context of transposase-coding gene domestication. First, while PB mostly mediates proper *Ifp2* transposition, it is also sometimes responsible for improper transposition that leads to neo-inserted elements that are difficult or impossible to re-mobilise during new rounds of transposition. Second, *pble* transposases might display strong preferences for insertion and genome rearrangements. Indeed, we noted that PGBD5 is highly expressed in the mammalian nervous system [20] and that current publicly available data (https://www.gtexportal.org/home/gene/PGBD5; https://www.proteinatlas.org/search/PGBD5) widely support this conclusion. However, these data concern mRNA expression and data regarding mRNA translation and protein expression will be required. Nevertheless, if acquiring a mechanism for triggering irreversible DNA rearrangements in the early steps of vertebrate evolution in the nervous system can be considered advantageous, then

PGBD5 seems to possess all the properties required to play such a role. The evolutionary history of the RAG1/RAG2 proteins [33] suggests that each time a domesticated transposase has emerged during evolution its domestication was concurrent with the domestication of its transposon targets. In the PGBD5 context, verifying that *pbles* are domesticated and are used as binding targets by PGBD5 for genome rearrangements will be challenging. Indeed, while PGBD5 is a highly conserved protein in vertebrates, the *pble* landscape in these genomes varies drastically from one host species to the next. In the human genome three *pbles* unrelated to PGBD5 are annotated: MER75, MER85 and *Looper*. In the mouse genome only one *pble* closely related to human *Looper* is annotated. In the zebrafish seven *pbles* that were not related to PGBD5 and to those present in human and mouse genomes, have been annotated. In the chicken genome no *pble* has been found so far [34,35]. It is possible that PGBD5 has been domesticated in order to mobilise multiple *pbles* for recombination. Its protein sequence conservation in chicken and the absence of *pble*s in this species suggests that it binds to other DNA binding targets, which may be related to the PGBD5-specific signal (PSS) sequences observed in human rhabdoid tumors [14].

Materials and methods

cDNA cloning of PGBD5 murine isoforms.

A single mouse brain (strain C57Bl6) was used for total RNA extraction using Tri-reagent (Sigma-Aldrich, St-Louis, MO, USA). cDNA synthesis was carried out using Omniscript RT kit and oligo dT primers (Qiagen, Valencia, CA, USA). PCR primers with appropriate flanking restriction sites were synthesized by Eurofins Genomics, Ebersberg, Germany. PCR was performed with Phusion High-Fidelity PCR Master Mix (ThermoScientific). Following agarose gel electrophoresis, PCR fragments were extracted (QIAquick gel extraction kit, Qiagen), submitted to enzyme restriction (*Eco*RI/*Xba*I for the long N-term isoform and *Eco*RI/*Xho*I for the short N-term isoform), purified (QIAquick PCR purification kit, Qiagen) and kept for cloning. Their sequence identity was verified by Sanger sequencing (Eurofins Genomics, Ebersberg, Germany). The primers used to amplify Mm523 (Accession N°: XM_006530804.1) isoforms are supplied in supplementary data 1a.

Integration assay.

Plasmid expression for transposases. The plasmids pCS2-PB and pCS2-PB.NLS-1-558 encode the V5 tagged PB transposases. Each cDNA was inserted into the multi-cloning site of the pCS2+ vector (Life Technologies, Paisley, UK) as described [36]. The plasmid pCS2-Mm523 encodes a two myc tagged PGBD5 isoform 524 amino acid residues in size. Mm523 cDNA was inserted into the multi-cloning site of a modified pCS2 vector with an in-frame N-term 5XMyc tag [37]. The plasmid pCS2-GFP plasmid was built by cloning the gene coding for the green fluorescent protein gene into the

multi-cloning site of the pCS2+ vector. pCS2-GFP was used as a negative control of transposition (i.e. absence of transposase expression).

Plasmids donor of transposon. The plasmid pBSK-IFP2-TIR5'-NeoR-TIR3' (supplementary data 1b) was built by introducing the IFP2 5' and 3' terminal regions (262 and 400 bp, respectively) into the pBluescript SK plasmid (pBSK). A cassette (NeoR) containing a SV40 promoter, the neomycin phosphotransferase ORF and a sv40 terminator was cloned between transposon ends as described [36]. NeoR was cloned in its middle using a BamHI site that was added to its sequence during DNA synthesis. The plasmid pBSK-NeoR was built by cloning the NeoR cassette into the multi-cloning site of a pBSK plasmid as described [38].

Integration assay in HeLa cells. Assays were monitored as described [36]. Briefly, each sample of 100000 cells in a well of a 24-well plates of plaque assays was co-transfected with JetPEI (Polyplus-transfection, Illkirch-Graffenstaden) and 400 ng DNA plasmid and with equal amounts of donor of NeoR cassette included or not within a transposon and transposase sources (1:1 ratio). Two days post-transfection, each cell sample was transferred to a cell culture dish (100 mm diameter) and selected with a culture medium containing 800 µg/mL G418 sulfate (Eurobio Scientific, Les Ulis) for 15 days. After two washing with 1X saline phosphate buffer, cell clones were fixed and stained overnight with 70% EtOH-0.5% methylene blue and colonies > 0.5 mm in diameter were counted. Experiments were performed at least twice in triplicate.

Integration assay in G401 cells. Assays were monitored as described [14]. Two clonal cell G401 lines were used. The first line was lentivirally transduced to constitutively express specific shRNA suppressing the expression of Hs524 PGBD5 [14]. The second line was modified as a control to constitutively express shRNA to target GFP which is not expressed, thereby preserving the endogenous expression of Hs524 PGBD5. Briefly, each sample of 100000 cells in a well of a 24-well plates of plaque assays was transfected with jetOptimus and 500 ng DNA plasmid pBSK-IFP2-TIR5'-NeoR-TIR3' as recommended by the supplier (Polyplus- transfection, Illkirch-Graffenstaden). Two days post-transfection, each cell sample was transferred to a cell culture dish (100 mm diameter) and selected with a culture medium containing 2 mg/mL G418 sulfate (Eurobio Scientific, Les Ulis) for 15 days. After two washing with 1X saline phosphate buffer, cell clones were fixed and stained overnight with 70% EtOH-0.5% methylene blue and colonies > 0.5 mm in diameter were counted. Experiments were performed at least twice in triplicate.

Cellular localization of green fluorescent protein-fusion proteins

Plasmid expression for transposase-GFP fusions. The plasmids pCS2-PB-GFP, pCS2-PB.1-558, pCS2-PB.NLS-1-558 and pCS2-Mm523-GFP were made as described [39].

Cell manipulation. HeLa cells were plated at a density of 5 x 10^4 cells per well in 1 cm^2 Lab-Tek™ chamber slides (Fisher Scientific, Waltham, MA, USA) and grown in DMEM (Gibco/Life Technologies, Paisley, UK) supplemented with 10 % heat inactivated fetal bovine serum (FBS, Eurobio, France) at 37 °C in a humidified atmosphere containing 5% CO2 for 48 h. Cells were transfected with 500 ng plasmid DNA and jetPEI™ (Polyplus Transfection, Illkirch, France) at an N/P ratio of 5 in DMEM 10% FBS following the Manufacturer's instructions. Cells were then incubated with the complexes for 4 h. The transfection medium was then discarded and replaced by fresh DMEM supplemented with 10% FBS before being incubated for 48 hours at 37°C.

Imaging. Cells on slides were fixed in 1X PBS/2% paraformaldehyde at RT for 15 min, and then permeabilised with PBS/1% (w/v) Triton-X100 for 10 min. The slides were washed three times for 5 min with 1x PBS. Nuclei were stained using Vectashield Vibrance "Antifade Mounting Medium (hardening) + DAPI" (Vector Laboratories, Burlingame CA, USA). All images of fluorescence were collected with an LSM 700 laser scanning microscope and the associated Zen software (Carl Zeiss, Oberkochen, Germany). All images shown correspond to one focal plane (0.5 μm). Images to be used for figures were pseudocolored by LSM Image browser software (Carl Zeiss, Thornwood, NY) and Photoshop (Adobe Systems, San Jose, CA) was on the resulting tiff files only to adjust for brightness and contrast.

Recovery of integration sites.

LAM-PCR and Illumina libraries. Integration assays were done to produce cell populations containing integrated copies of the donor transposon. Fifteen days post-transfection, cell clones were harvested for genomic DNA preparation using the DNeasy kit (Qiagen, Hilden, Germany). Linear amplification-mediated PCR (LAM-PCR) was performed to amplify the vector-genomic DNA junctions of *Ifp2* vectors as described [40]. All PCR were done using the high fidelity Q5 DNA Polymerase (New England Biolabs, Ipswich, MA). For both approaches, 1 μg DNA was used for twice 50 rounds of linear amplification using a biotinylated primer anchored near one end of the NeoR cassette to enrich DNA species containing transposon-chromosomal DNA junctions (for sequences of (B)-NeoR 5' and 3' primers, see supplementary data 1c). One reaction was done per ends. The single-stranded products were immobilized on streptadivin-coated magnetic beads (Dynabeads M-280 Streptavidin, Invitrogen, Carlsbad, CA). All subsequent steps were performed on the magnetic bead-bound DNA. Two washes with water followed each step. Second strand

synthesis was performed with random hexamer primers (Roche, Basel, Switzerland) using Klenow DNA polymerase (New England Biolabs, Ipswich, MA). The double-stranded DNA was split in two batches and subjected to restriction digests with *DpnI* for the first one and *Pci*I, *Nco*I and *Bsp*HI for the second one using restriction enzymes. The DNA fragments with a CG-3' or a CATG-3' overhang ends were ligated to linkers displaying appropriate overhang ends and made from annealed oligonucleotides (supplementary data 1c).

To increase the specificity of the full process, an initial PCR was done using one biotinylated primer anchored within the 5' or 3' region of the transposon donor and one primer anchored within the linker (for sequences of (B)-TIR-UTR 5' and 3', and LC1 primers, see supplementary data 1c). PCR products were immobilized on streptadivin-coated magnetic beads and purified as described above. Next, the bead-bound DNA was subjected to a nested PCR using nested primers anchored within transposon ends and within linkers (supplementary data 1c). Final PCR products were purified, quantified and gathered in equimolar DNA amounts for each transposon vector (4 populations of LAM-PCR products) before being used to make Illumina libraries using NEBNext® Ultra™ II DNA Library Prep Kit for Illumina® and NEBNext Multiplex Oligos for Illumina (New England Biolabs, Ipswich, MA). Fragment size selection, library quality control and Illumina sequencing (MiSeq 250 nucleotides, TruSeq SBS Kit v3) were achieved at the Plateforme de Séquençage Haut Débit I2BC (Gif-sur-Yvette, France). DNA quantities were monitored at various steps in the procedure with the Qubit® dsDNA (Molecular Probes, Eugene, USA).

Computer analysis. Trimmomatic [41] was used to filter Miseq reads using default parameters, except for SLIDINGWINDOW:5:20 and MINLEN:100. The purpose of the following steps was to recover chromosome-inserted DNA fragment junctions taking into account the plasmid backbone regions located 100-bp upstream and downstream the *Ifp2*-NeoR transposon. Filtered reads were first mapped to the sequence of plasmid backbone minus the 100-bp regions flanking on both sides the *Ifp2*-NeoR transposon with bwa-mem using default parameters [42]. Unmapped reads were then extracted reads using SAMtools view with parameters -b -f 4 [43] and bamToFastq from the BEDTools suite using default parameters [44]. Recovered unmapped reads were aligned using bwa-mem against a bwa bank gathering the sequences of hg38 chromosomes plus those of the *Ifp2*-NeoR transposon flanked by the 100-bp plasmid backbone regions on both sides (supplementary data 1d). Default parameters were used excepted for -w 1 and -r 1. The bam files resulting from each dataset alignment were analysed with Lumpy in order to identify split reads [45]. The parameters were -e -mw 2 -tt 0.0 and back_distance:20,weight:1,id:lumpy_v1,min_mapping_threshold:20. Structural variants (SV) characterized by "BND" for the broken end notations and displaying for each of them an SV with two positions, one genomic and one on the transposon, were extracted using a house

python program (https://github.com/Leelouh/lumpy2site). Results were filtered taking into account a difference below 3 between the transposon breakpoint calculated by Lumpy and the maximal spread of read alignments in the transposon donor sequence for each integration event. Each TSD nucleotide motif at insertion site was obtained after extracting 10-bp sequences before and after the breakpoint in the chromosome sequences.

Gene ontology (GO) analyses were focused mostly on protein coding genes and those encoding long non-coding RNA (lncRNA). We used hg38 gene annotations from UCSC. Gene ontology was first investigated using DAVID (https://david.ncifcrf.gov/) and AmiGO2 (http://amigo.geneontology.org/amigo) to assess term enrichment. This was followed up by the Cytoscape plugin ClueGO [46,47].

Access of publicly available data

Sequences corresponding to *Ifp2*, *Sleeping Beauty* and *TcBuster* insertion sites in HEK 293 cells [23] were downloaded from public databases using accession numbers JS717545 to JS799249. Sequences corresponding to *Ifp2* insertion sites in HCT116 cells [15] were recovered at https://www.genetics.org/content/suppl/2012/01/03/genetics.111.137315.DC1. Sequences corresponding to *Ifp2* and *Sleeping Beauty* insertion sites in CD4+ cells [26] were recovered in the GSE58744 at https://www.ncbi.nlm.nih.gov/geo/query/acc.cgi?acc=GSM1419000 and https://www.ncbi.nlm.nih.gov/geo/query/acc.cgi?acc=GSM1419001. For the last two sources, the positions of insertion sites were transformed in hg38 using liftover at https://genome.ucsc.edu/cgi-bin/hgLiftOver. All sites mapped in hg38 were supplied in supplementary Table 4.

PWMTrain [48] at https://ccg.epfl.ch/pwmtools/pwmtrain.php was used to calculate the position-specific weight matrix of *TcBuster* insertion sites using available data [23]. The numbers and the positions of putative insertion sites in hg38 for *pbles* (TTAA), *sleeping beauty (*TA) and *TcBuster* were calculated using PWMScan [48] at https://ccg.epfl.ch//pwmtools/pwmscan.php.

The list of 6985 neuron genes in hg19 was recovered in supplemental data of [31] and was updated to hg38. 131 genes were removed. They corresponded to artefactual genes coding nc RNA that were withdrawn in hg 38. DNAse1 map for HeLa and HEK293 cells were recovered at http://hgdownload.soe.ucsc.edu/wgEncodeAwgDnaseUwdukeHelas3UniPk.narrowPeak.gzgoldenPath/hg19/encodeDCC/wgEncodeOpenChromDnase/, files and http://hgdownload.soe.ucsc.edu/goldenPath/hg19/encodeDCC/wgEncodeAwgDnaseUniform/wgEncodeAwgDnaseUwdukeHelas3UniPk.narrowPeak.gz. They were updated in hg38 using liftover.

Values in graphs were medians, quartiles 1 and 3 and spread of experiments done at least twice in triplicate. Shapiro-Wilk tests were used to confirm the normality of each set of samples, t-test to analyse distribution differences between experimental samples, Chi2 test to analyse differences

between an experimental distribution and a theoretical one, and logarithmic distribution test to analyse enrichments using free tools and tutorials available at http://www.anastat.fr/outils.php. Permutation tests (10,000 per test) were computed using in-house bash programs that accounted the distribution in TA and TTAA motifs in hg38. The normality of each distribution of permuted results was verified using a Shapiro-Wilk test using free tools and tutorials available at http://www.anastats.fr/outils.php. When the distributions were normal, probabilities were calculated from Z score at https://www.fourmilab.ch/rpkp/experiments/analysis/zCalc.html. When they were not normal, the distributions were used to determine the 1 and 0.1% thresholds at both tails and the observed values were positioned in regards to those values.

Data deposition.

All raw and processed data are available through the European Nucleotide Archive under accession number PRJEB36226, PRJEB36229, PRJEB41045 and PRJEB41053. Files describing the annotation of insertion sites copies in the hg38 release are supplied as supplementary Tables 1, 2 and 3.

Acknowledgments

This work was supported by the C.N.R.S., the I.N.R.A., and the GDR CNRS 2157. It also received funds from a research program grants from the Ligue Nationale Contre le Cancer, the Merck foundation, and the French National Society of Gastroenterology. Laura Helou holds a PhD fellowship from the Région Centre Val de Loire. We acknowledge the high-throughput sequencing facility of I2BC for its sequencing and bioinformatics expertise. Alex Kentsis is a consultant for Novartis and is supported by the National Cancer Institute grants R01 CA214812 and P30 CA008748. Yves Bigot, who was in charge of the achievement of this project does not have to thank the French National Research Agency for its financial support but he kindly thanks it for the excellent reviews embellished with arguments based on scientific and cultural novelties in the expertise of his yearly application file during the last decade.

Appendix A: Supplemental data

Supplementary data 1. Transposon donor sequences and primers used in the study.

Supplementary Table 1. (a) Inventory of *Ifp2*-chromosome junctions resulting from integration events mediated by PB. Transposon breakpoints located at positions 102 and 2220, 103 and 2219, 104 and 2218, and 105 and 2217 had a TSD displaying a DTAA, DDAA, DDBA or DDBB nucleotide motif (IUPAC nucleotide code; blue bars in Fig. 3a). Those at positions 101 and 2221, 100 and 2222, 99 and 2223, and 98 and 2224 (red bars in Fig. 3a) displayed a TTAA TSD with upstream or downstream 0 nucleotide, one nucleotide, a dinucleotide or a trinucleotide that were identical in the plasmid backbone and the chromosome. As the origin of this specific trait could not be differentiated with a probability threshold below 1%, all junctions were considered in the analysis as originating from proper integration events. **(b) Inventory of chromosomal site in which *Ifp2* insertions were found several times.** Insertions corresponding to a single putative integration event were highlighted in cyan blue and their duplicated TSD was highlighted in green. Integration events corresponding to proper transposon ends were typed in black while those with improper ends were typed in red.

Supplementary Table 2. (a) Inventory of *Ifp2*-chromosome junctions resulting from integration events mediated by PB.NLS-1-558. Transposon breakpoints located at positions 102 and 2220, 103 and 2219, 104 and 2218, and 105 and 2217 had a TSD displaying a DTAA, DDAA, DDBA or DDBB nucleotide motif (IUPAC nucleotide code; blue bars in Fig. 3b). Those at positions 101 and 2221, 100 and 2222, 99 and 2223, and 98 and 2224 (red bars in Fig. 3b) displayed a TTAA TSD with upstream or downstream 0 nucleotide, one nucleotide, a dinucleotide or a trinucleotide that were identical in the plasmid backbone and the chromosome. As the origin of this specific trait could not be differentiated with a probability threshold below 1%, all junctions were considered in the analysis as originating from proper integration events. **(b) Inventory of chromosomal site in which *Ifp2* insertions were found several times.** Insertions corresponding to a single putative integration event were highlighted in cyan blue and their duplicated TSD was highlighted in green. Integration events corresponding to proper transposon ends were typed in black while those with improper ends were typed in red.

Supplementary Table 3. (a) Inventory of *Ifp2*-chromosome junctions resulting from integration events mediated by Mm523. Transposon breakpoints located at positions 102 and 2220, 103 and 2219, 104 and 2218, and 105 and 2217 had a TSD displaying a DTAA, DDAA, DDBA or DDBB nucleotide motif (IUPAC nucleotide code; blue bars in Fig. 3c) displayed a TTAA

TSD with upstream or downstream 0 nucleotide, one nucleotide, a dinucleotide or a trinucleotide that were identical in the plasmid backbone and the chromosome. As the origin of this specific trait could not be differentiated with a probability threshold below 1%, all junctions were considered in the analysis as originating from proper integration events. **(b) Inventory of chromosomal site in which *Ifp2* insertions were found several times.** Insertions corresponding to a single putative integration event were highlighted in cyan blue and their duplicated TSD was highlighted in green. Integration events corresponding to proper transposon ends were typed in black while those with improper ends were typed in red.

Supplementary Table 4. (a) Inventory of *Ifp2*-chromosome junctions resulting from integration events mediated by Hs524 in G401 cells. Transposon breakpoints located at positions 102 and 2220, 103 and 2219, 104 and 2218, and 105 and 2217 had a TSD displaying a DTAA, DDAA, DDBA or DDBB nucleotide motif (IUPAC nucleotide code; blue bars in Fig. 3c) displayed a TTAA TSD with upstream or downstream 0 nucleotide, one nucleotide, a dinucleotide or a trinucleotide that were identical in the plasmid backbone and the chromosome. As the origin of this specific trait could not be differentiated with a probability threshold below 1%, all junctions were considered in the analysis as originating from proper integration events. **(b) Inventory of chromosomal site in which *Ifp2* insertions were found several times.** Insertions corresponding to a single putative integration event were highlighted in cyan blue and their duplicated TSD was highlighted in green. Integration events corresponding to proper transposon ends were typed in black while those with improper ends were typed in red.

Supplementary Table 5. Chromosomal positions mapped here in hg38 for Ifp2 insertion sites in HEK293 (a), HCT116 (b) and CD4+ (c) cells, sleeping beauty in HEK293 (d) and CD4+ (e), and TcBuster in HEK293 (f).

References

1. Piégu, B., Bire; S., Arensburger, P., Bigot, Y. (2016) A survey of transposable element classification systems--a call for a fundamental update to meet the challenge of their diversity and complexity. Mol. Phylogenet. Evol. 86, 90-109.

2. Arensburger, P., Piégu, B., Bigot, Y. (2016) The future of transposable element annotation and their classification in the light of functional genomics - what we can learn from the fables of Jean de la Fontaine? Mob. Genet. Elements. 6, e1256852.

3. Arkhipova, I.R. (2017) Using bioinformatic and phylogenetic approaches to classify transposable elements and understand their complex evolutionary histories. Mob. DNA. 8, 19.

4. Goerner-Potvin, P., Bourque, G. (2018) Computational tools to unmask transposable elements. Nat. Rev. Genet. 19, 688-704.

5. Bouallègue, M., Rouault, J.D., Hua-Van, A., Makni, M., Capy, P. (2017) Molecular Evolution of piggyBac Superfamily: From Selfishness to Domestication. Gen. Biol. Evol.9, 323-339.

6. Cary, L.C., Goebel, M., Corsaro, B.G., Wang, H.G., Rosen, E., Fraser, M.J. (1989) Transposon mutagenesis of baculoviruses: analysis of Trichoplusia ni transposon IFP2 insertions within the FP-locus of nuclear polyhedrosis viruses. Virology. 172, 156-169.

7. Yusa, K. (2015) piggyBac Transposon. Microbiol. Spectr. 3, MDNA3-0028-2014.

8. Chen, Q., Luo, W., Veach, R.A., Hickman, A.B., Wilson, M.H., Dyda, F. (2020) Structural basis of seamless excision and specific targeting by piggyBac transposase. Nat Commun 11, 3446.

9. Morellet, N., Li, X., Wieninger, S.A., Taylor, J.L., Bischerour, J., Moriau, S., Lescop, E., Bardiaux, B., Mathy, N., Assrir, N., Bétermier, M., Nilges, M., Hickman, A.B., Dyda, F., Craig, N.L., Guittet, E. (2018) Sequence-specific DNA binding activity of the cross-brace zinc finger motif of the piggyBac transposase. Nucl. Acids. Res. 46, 2660-2677.

10. Sharma, R., Nirwal, S., Narayanan, N., Nair, D.T. (2018) Dimerization through the RING-Finger domain attenuates excision activity of the piggyBac transposase. Biochemistry. 57, 2913-2922.

11. Keith, J.H., Fraser, T.S., Fraser, M.J.Jr. (2008) Analysis of the piggyBac transposase reveals a functional nuclear targeting signal in the 94 c-terminal residues. BMC. Mol. Biol. 9, 72.

12. Hong, J.B., Chou, F.J., Ku, A.T., Fan, H.H., Lee, T.L., Huang, Y.H., Yang, T.L., Su, I.C., Yu, I.S., Lin, S.W., Chien, C.L., Ho, H.N., Chen, Y.T. (2014) A nucleolus-predominant piggyBac transposase, NP-mPB, mediates elevated transposition efficiency in mammalian Cells. PLoS. One. 9, e89396.

13. Luo, W., Galvan, D.L., Woodard, L.E., Dorset, D., Levy, S., Wilson, M.H. (2017) Comparative analysis of chimeric ZFP-, TALE- and Cas9-piggyBac transposases for integration into a single locus in human cells. Nucl. Acids. Res. 45, 8411-8422.

14. Henssen, A.G., Koche, R., Zhuang, J., Jiang, E., Reed, C., Eisenberg, A., Still, E., MacArthur, I.C., Rodríguez-Fos, E., Gonzalez, S., Puiggròs, M., Blackford, A.N., Mason, C.E., de Stanchina, E., Gönen, M., Emde, A.K., Shah, M., Arora, K., Reeves, C., Socci, N.D., Perlman, E., Antonescu, C.R;, Roberts, C.W.M., Steen, H., Mullen, E., Jackson, S.P., Torrents, D., Weng, Z., Armstrong, S.A., Kentsis, A. (2017) PGBD5 promotes site-specific oncogenic mutations in human tumors. Nat. Genet. 49, 1005-1014.

15. Wang, H., Mayhew, D., Chen, X., Johnston, M., Mitra, R.D. (2012) "Calling cards" for DNA-binding proteins in mammalian cells. Genetics. 190, 941-949.

16. Li, M.A., Pettitt, S.J., Eckert, S., Ning, Z., Rice, S., Cadiñanos, J., Yusa, K., Conte, N., Bradley, A. (2013) The piggyBac transposon displays local and distant reintegration preferences and can cause mutations at noncanonical integration sites. Mol. Cell. Biol. 33, 1317-1330.

17. Thorvaldsdóttir, H., Robinson, J.T., Mesirov, J.P. (2013) Integrative Genomics Viewer (IGV): high-performance genomics data visualization and exploration. Brief. Bioinformatics. 14, 178-192.

18. Elick, T.A., Lobo, N., Fraser, M.J.Jr. (1997) Analysis of the cis-acting DNA elements required for piggyBac transposable element excision. Mol. Gen. Genet. 255, 605-610.

19. Mitra, R., Fain-Thornton, J., Craig, N.L. (2008) piggyBac can bypass DNA synthesis during cut and paste transposition. EMBO. J. 27, 1097-1109.

20. Pavelitz, T., Gray, L.T., Padilla, S.L., Bailey, A.D., Weiner, A.M. (2013) PGBD5: a neural-specific intron containing piggyBac transposase domesticated over 500 million years ago and conserved from cephalochordates to humans. Mob. DNA. 4, 23-39.

21. Henssen, A.G., Henaff, E., Jiang, E., Eisenberg, A.R., Carson, J.R., Villasante, C.M., Ray, M., Still, E., Burns, M., Gandara, J., Feschotte, C., Mason, C.E., Kentsis, A. (2015) Genomic DNA transposition induced by human PGBD5. Elife. 4, e10565.

22. Lohe, A.R., Timmons, C., Beerman, I., Lozovskaya, E.R., Hartl, D.L. (2000) Self-inflicted wounds, template-directed gap repair and a recombination hotspot. Effects of the mariner transposase. Genetics. 154, 647-656.

23. Woodard, L.E., Li, X., Malani, N., Kaja, A., Hice, R.H., Atkinson, P.W., Bushman, F.D., Craig, N.L., Wilson, M.H. (2012) Comparative analysis of the recently discovered hAT transposon TcBuster in human cells. PLoS. One. 7, e42666.

24. Wilson, M.H., Coates, C.J., George, A.L.Jr. (2007) PiggyBac transposon-mediated gene transfer in human cells. Mol. Ther. 15, 139-145.

25. Huang, X., Guo, H., Tammana, S., Jung, Y.C., Mellgren, E., Bassi, P., Cao, Q., Tu, Z.J., Kim, Y.C., Ekker, S.C., Wu, X., Wang, S.M., Zhou, X. (2010) Gene transfer efficiency and genome-wide integration profiling of Sleeping Beauty, Tol2, and piggyBac transposons in human primary

T cells. Mol. Ther. 18, 1803-1813.

26. Gogol-Döring, A., Ammar, I., Gupta, S., Bunse, M., Miskey, C., Chen, W., Uckert, W., Schulz, T.F., Izsvák, Z., Ivics, Z. (2016) Genome-wide profiling reveals remarkable parallels between insertion site selection properties of the MLV retrovirus and the piggyBac transposon in primary human CD4(+) T cells. Mol Ther. 24, 592-606.

27. Landry, J.J., Pyl, P.T., Rausch, T., Zichner, T., Tekkedil, M.M., Stütz, A.M., Jauch, A., Aiyar, R.S., Pau, G., Delhomme, N., Gagneur, J., Korbel, J.O., Huber, W., Steinmetz, L.M. (2013) The genomic and transcriptomic landscape of a HeLa cell line. G3 (Bethesda). 3, 1213-1224.

28. Adey, A., Burton, J.N., Kitzman, J.O., Hiatt, J.B., Lewis, A.P., Martin, B.K., Qiu, R., Lee, C., Shendure, J. (2013) The haplotype-resolved genome and epigenome of the aneuploid HeLa cancer cell line. Nature. 500, 207-211.

29. Lin, Y.C., Boone, M., Meuris, L., Lemmens, I., Van Roy, N., Soete, A., Reumers, J., Moisse, M., Plaisance, S., Drmanac, R., Chen, J., Speleman, F., Lambrechts, D., Van de Peer, Y., Tavernier, J., Callewaert, N. (2014) Genome dynamics of the human embryonic kidney 293 lineage in response to cell biology manipulations. Nat Commun. 5, 4767.

30. Liu, Y., Mi, Y., Mueller, T., Kreibich, S., Williams, E.G., Van Drogen, A., Borel, C., Frank, M., Germain, P.L., Bludau, I., Mehnert, M., Seifert, M., Emmenlauer, M., Sorg, I., Bezrukov, F., Bena, F.S., Zhou, H., Dehio, C., Testa, G., Saez-Rodriguez, J., Antonarakis, S.E., Hardt, W.D., Aebersold, R. (2019) Multi-omic measurements of heterogeneity in HeLa cells across laboratories. Nat Biotechnol. 37, 314-322.

31. Negi, S.K., Guda, C. (2017) Global gene expression profiling of healthy human brain and its application in studying neurological disorders. Sci. Rep.7, 897.

32. Zylka, M.J., Simon, J.M., Philpot, B.D. (2015) Gene length matters in neurons. Neuron. 86, 353-355.

33. Zhang, Y., Cheng, T.C., Huang, G., Lu, Q., Surleac, M.D., Mandell, J.D., Pontarotti, P., Petrescu, A.J., Xu, A., Xiong, Y., Schatz, D.G. (2019) Transposon molecular domestication and the evolution of the RAG recombinase. Nature. 569, 79-84.

34. Guizard, S., Piégu, B., Arensburger, P., Guillou, F., Bigot, Y. (2016) Deep landscape update of dispersed and tandem repeats in the genome model of the red jungle fowl, Gallus gallus, using a series of de novo investigating tools. BMC Genomics. 17, 659.

35. Kapusta, A., Suh, A. (2017) Evolution of bird genomes-a transposon's-eye view. Ann. N. Y. Acad. Sci. 1389, 164-185.

36. Bire, S., Ley, D., Casteret, S., Mermod, N., Bigot, Y., Rouleux-Bonnin, F. (2013) Optimization of the piggyBac transposon using mRNA and insulators: toward a more reliable gene delivery system. PLoS. One. 8, e82559.

37. Travnickova-Bendova, Z., Cermakian, N., Reppert, S.M., Sassone-Corsi, P. (2002) Bimodal regulation of mPeriod promoters by CREB-dependent signaling and CLOCK/BMAL1 activity. Proc. Natl. Acad. Sci. USA. 99, 7728-7733.

38. Bire, S., Casteret, S., Piégu, B., Beauclair, L., Moiré, N., Arensbuger, P., Bigot, Y. (2016) Mariner Transposons Contain a Silencer: Possible Role of the Polycomb Repressive Complex 2. PLoS. Genet. 12, e1005902.

39. Demattei, M.V., Hedhili, S, Sinzelle, L., Bressac, C., Casteret, S., Moiré, N., Cambefort, J., Thomas, X., Pollet, N., Gantet, P., Bigot, Y. (2011) Nuclear importation of Mariner transposases among eukaryotes: motif requirements and homo-protein interactions. PLoS One. 6, e23693.

40. Bartholomae, C.C., Glimm, H., von Kalle, C., Schmidt, M. (2012) Insertion site pattern: global approach by linear amplification-mediated PCR and mass sequencing. Meth. Mol. Biol. 859, 255-265.

41. Bolger, A.M., Lohse, M., Usadel, B. (2014) Trimmomatic: a flexible trimmer for Illumina sequence data. Bioinformatics. 30, 2114-2120.

42. Li, H., Durbin, R. (2010) Fast and accurate long-read alignment with Burrows–Wheeler transform, Bioinformatics. 26, 589-595.

43. Li, H., Handsaker, B., Wysoker, A., Fennell, T., Ruan, J., Homer, N., Marth, G., Abecasis. G., Durbin, R., and 1000 Genome Project Data Processing Subgroup. (2009) The Sequence alignment/map (SAM) format and SAMtools. Bioinformatics. 25, 2078-2079.

44. Quinlan, A.R., Hall, I.M. (2010) BEDTools: a flexible suite of utilities for comparing genomic features. Bioinformatics. 26, 841-842.

45. Layer, R.M., Chiang, C., Quinlan, A.R., Hall, I.M. (2014) LUMPY: a probabilistic framework for structural variant discovery. Gen. Biol 15, R84.

46. Bindea, G., Mlecnik, B., Hackl, H., Charoentong, P., Tosolini, M., Kirilovsky, A., Fridman, W.F., Pagès, F., Trajanoski, Z., Galon, J. (2009) ClueGO: a Cytoscape plug-in to decipher functionally grouped gene ontology and pathway annotation networks. Bioinformatics. 25, 1091-1093.

47. Mlecnik, B., Galon, J., Bindea, G. (2018) Comprehensive functional analysis of large lists of genes and proteins. J. Proteomics. 171, 2-10.

48. Ambrosini, G., Groux, R., Bucher, P. (2018) PWMScan: A Fast Tool for Scanning Entire Genomes with a Position-Specific Weight Matrix. Bioinformatics. 34, 2483-2484.

Legends

Fig. 1. Cellular localization of GFP fusions in HeLa cells transiently transfected with a vector expressing GFP (a, b, c), PB-GFP (d, e, f), PB.1-558-GFP (g, h, i) and PB.NLS-1-558-GFP (j, k, l). The left panels (a, d, g, j) show GFP fluorescence, the middle panels (b, e, h, k)) show the nuclear genomic DNA staining by Hoechst 33342, the right panels (c, f, I, l) correspond to merge pictures.

Fig. 2. Box plot representations of integration assay results. (a) impact of the two PB variants (PB.1-558 and PB.NLS-1-558), PB and GFP on the rate of random integration of a NeoR cassette. (b) rates of NeoR clones resulting from the integration of *Ifp2*-NeoR when recombination was mediated by the two PB variants, PB and GFP. (c) rates of NeoR clones resulting from the integration of *Ifp2*-NeoR when recombination was mediated by PB.NLS-1-558, PB and GFP and corrected by the rate of toxicity of each protein calculated in (a). In (b) and (c), integration rates were expressed in rate NeoR clones that were normalized using controls done with GFP. In each plot, the red lines represented the median and the standard deviation, respectively.

Fig. 3. Number and location of transposon breakpoints in *pble* sequences after transposition into chromosomes. Histogram distributions of Ifp2-NeoR extremities transposed by PB (a), PB.NLS-1-558 (b), Mm523 (c) and Hs524 (d) (detailed in supplementary Tables 1 to 4). Red bars indicated insertion events with perfectly conserved TSD and TIR while blue bars located those in which TIR were perfectly conserved but the TSD did not correspond to a canonical TTAA at the outermost extremities of pbles. Black bars represented breakpoints within the transposon sequence and within plasmid backbone sequences juxtaposed to the transposon. Each bar corresponded to the number of junctions found at a single nucleotide position. Green boxes located the position of primers anchored within the transposon sequence and used at the last step of LAM-PCR. These graphics described the relative importance of wounds at transposon ends under our experimental conditions. However, they could not allow calculating wound rates at each of both ends due to the fact that the final LAM-PCR products in each dataset came from the gathering of several LAM-PCR reactions.

Fig. 4. Sequence features of the *Ifp2* transposase (PB) variants and two Mm523-like PGBD5 isoforms. (a) Protein sequence alignment of Ifp2 transposase (PB) with two murine and human domesticated PGBD5 proteins corresponding to the orthologous Hs524 and Mm523 isoforms. (b) Sequence features of PB.NLS-1-558. Secondary structure predictions calculated with psipred (http://bioinf.cs.ucl.ac.uk/psipred/) and Jpred4 (http://www.compbio.dundee.ac.uk/jpred/) were

highlighted in pink for α-helices and in orange for β-strands. The three proteins share two domains: a N-terminal domain that was few structured, with an acid pI (boxed regions) and repeated acid motifs (in red letters), a domain of ~400 amino acid residues that display a basic pI. PB contained a third C-terminal domain, the CRD, that contains cysteins (highlighted in green) able to assemble zinc finger folds. Aspartic residues inactivating the recombinase catalytic activity were bolded and highlighted in yellow [17,21]. The PB NLS and the putative NLS in PGBD5 isoforms were underlined and typed in green.

Fig. 5. Graphic representations of integration assay results. (a) impact of Mm523 on the rate of random integration of a NeoR cassette. (b) rates of integration of an *Ifp2*-NeoR when recombination was mediated by PB and Mm523 in HeLa cells, and Hs524 in G401 cells. Integration rates were expressed in rate NeoR clones that were normalized using controls done with GFP (green). In each plot, the red lines represented the median and the standard deviation, respectively.

Fig. 6. Features of transposon breakpoints in Ifp2 transposed by PB (a), PB.NLS-1-558 (b), Mm523 (c) and Hs524 (d). Black bars corresponded to percentages of breakpoints located within the plasmid backbone flanking the transposon or those located within inner transposon regions (from the position 2 in TIR to the primer used for the LAM-PCR). Red bars corresponded to those within transposons that displayed intact canonical TTAA TSD and TIRs. Blue bars corresponded to *pbles* displaying noncanonical TSD but intact TIRs.

Fig. 7. Proportions of Ifp2 insertions mediated by PB, PB.NLS-1-558, Mm523 and Hs524 in intragenic regions (a) and regions containing TSS (b) taking into account the five gene categories: protein-coding genes, ncRNA-coding genes, miRNA-coding genes, pseudogenes and uncharacterized genes. Black bars indicated the expect percentage in a random distribution.

Fig. 8. Venn diagram representations of intragenic regions overlapped by insertion site-containing regions (± 1000 bp) between transposition assays done with PB, PB.NLS-1-558, Mm523 and Hs524 (a) and with PB in HeLa, HEK293, HCT116 and CD4+ cells (b). The numbers of intragenic regions specific of datasets were italicized and typed in grey. Those shared by all datasets were typed in orange.

Table 1. Presence of canonic TTAA TSD and-or TIR among transposon/chromosome junctions resulting from LAM-PCR products and originating from events mediated by PB variants.

Transposase source	Transposon source	Proper TSD and TIR	Proper TSD improper TIR	Improper TSD/proper TIR	Improper TSD and TIR
PB	*Ifp2*-NeoR	96.7 % (7370)	1.05 % (78)	1.05 % (80)	1.2 % (95)
PB-NLS-1-558	*Ifp2*-NeoR	19.0 % (98)	2.5 % (13)	3.1 % (16)	75.4 % (388)

Table 2. Presence of canonic TTAA TSD and-or TIR among transposon/chromosome junctions resulting from LAM-PCR products and originating from events mediated by Mm523 and Hs524.

Transposase source	Transposon source	Proper TSD and TIR	Proper TSD improper TIR	Improper TSD/proper TIR	Improper TSD and TIR
Mm523 PGBD5	*Ifp2*-NeoR	10.0 % (147)	5.4 % (80)	4.3 % (64)	80.3 % (1188)
Hs524 PGBD5	*Ifp2*-NeoR	4.6 % (48)	2.1 % (22)	1.3% (14)	92.0 % (967)

Table 3. Number of chromosomal sites in common in each dataset pair and their statistical consitency in permutation tests.

Feature of dataset 1			Feature of dataset 2					Random permutations features			
Cell line 1	Transposon 1	Transposase 1	Cell line 2	Transposon 2	Transposase 2	Window around insertion sites (±) in both datasets	Number of sites observed	Average number of sites expected per chance	Standard deviation	Z score	Probability = H0 was no differences between obs. and exp.
HeLa	*Ifp2*	PB	HeLa	*Ifp2*	PB.NLS-1-558	0	1	N.A.	N.A.	N.A.	p<0.001
HeLa	*Ifp2*	PB	HeLa	*Ifp2*	PB.NLS-1-558	1000	37	N.A.	N.A.	N.A.	p<0.001
HeLa	*Ifp2*	PB	HeLa	*Ifp2*	Mm523-PGBD5	0	83	N.A.	N.A.	N.A.	p<0.001
HeLa	*Ifp2*	PB	HeLa	*Ifp2*	Mm523-PGBD5	1000	175	N.A.	N.A.	N.A.	p<0.001
HeLa	*Ifp2*	PB	G401	*Ifp2*	Hs524-PGBD5	0	24	N.A.	N.A.	N.A.	p<0.001
HeLa	*Ifp2*	PB	G401	*Ifp2*	Hs524-PGBD5	1000	42	N.A.	N.A.	N.A.	p<0.001
HeLa	*Ifp2*	PB	HEK293	*Ifp2*	PB	0	21	N.A.	N.A.	N.A.	p<0.001
HeLa	*Ifp2*	PB	HEK293	*Ifp2*	PB	1000	471	260.162	17.0215	12.3865	0
HeLa	*Ifp2*	PB	HCT116	*Ifp2*	PB	0	238	67.01	8.4329	20.2763	0
HeLa	*Ifp2*	PB	HCT116	*Ifp2*	PB	1000	2387	N.A.	N.A.	N.A.	p<0.006
HeLa	*Ifp2*	PB	CD4+	*Ifp2*	PB	0	24	N.A.	N.A.	N.A.	p<0.001
HeLa	*Ifp2*	PB	CD4-	*Ifp2*	PB	1000	213	97.684	10.2987	11,197	0
HEK293	*Ifp2*	PB	HCT116	*Ifp2*	PB	0	391	N.A.	N.A.	N.A.	p<0.001
HEK293	*Ifp2*	PB	HCT116	*Ifp2*	PB	1000	6600	5419.484	93.3269	12.0060	0
HEK293	*Ifp2*	PB	CD4+	*Ifp2*	PB	0	362	N.A.	N.A.	N.A.	p<0.001
HEK293	*Ifp2*	PB	CD4+	*Ifp2*	PB	1000	752	N.A.	N.A.	N.A.	p<0.001
HCT116	*Ifp2*	PB	CD4+	*Ifp2*	PB	0	16	81.825	9.0919	17.5073	0
HCT116	*Ifp2*	PB	CD4+	*Ifp2*	PB	1000	5235	2213.501	50.9891	59.2576	0
HEK293	*Sleeping Beauty*	SB	CD4+	*Sleeping Beauty*	SB	0	3	N.A.	N.A.	N.A.	p>0.083
HEK293	*Sleeping Beauty*	SB	CD4+	*Sleeping Beauty*	SB	1000	385	349.967	19.09	1.8350	p=0.034

N.A., not appropriated to use a Z-test as the distribution of the 1000 permutations results did not fulfil normality in a Shapiro-Wilk test. In the most right column is typed in red probabilities supporting that there was no difference at a threshold of 0.01.

Table 4

Table 4a. Rate of regions containing insertion sites in genes and neuron genes in hg38

1, Dataset features: cells, transposon / transposase sources	2, No of different ISCR*	3, No & % of different ISCR overlapping a gene***	4, No of genes overlapped by ISCR**	5, No & % of different ISCR overlapping a neuron gene***	6, No & % of neuron genes among genes overlapped by ISCR**	7, p****
HeLa, *Ifp2* / PB	7,623	5,060 (66.4%)	4,663	2,231 (29.2%)	1,587 (34.0%)	2.1×10^{-82}
HeLa, *Ifp2*/PB.NLS-1-558	516	327 (63.2%)	376	123 (23.8%)	123 (37.6%)	2.5×10^{-6}
HeLa, *Ifp2* / Mm523	1,479	863 (58.4%)	956	321 (21.7%)	303 (31.7 %)	3.1×10^{-11}
G401, *Ifp2* / Hs524	1052	665 (63.2%)	740	279 (26.5%)	258 (38.8%)	1.3×10^{-14}
HEK293, *Ifp2*/PB [22]	21,967	15,226 (69.3%)	9,370	7,173 (32.6%)	3,032 (32.4%)	1.9×10^{-150}
HCT116, *Ifp2*/PB [14]	172,866	113,648 (67.7%)	23,578	49,688 (28.8%)	5,945 (25.3%)	1.3×10^{-88}
CD4+, *Ifp2* / PB [25]	8,954	6,940 (77.5%)	5,763	3,134 (35.0%)	1,903 (33.0%)	6.2×10^{-89}
HCT116, *sleeping beauty*/SB [14]	28,490	17,534 (61.54%)	10,460	7,776 (27.3%)	3,229 (30.9%)	2.5×10^{-128}
CD4+, *sleeping beauty* /SB [25]	8,290	5,441 (64,63%)	5,133	2,406 (29.0%)	1,750 (34.1%)	2.9×10^{-93}
HCT116, *TcBuster*/ TCBUSTER [14]	17,227	11,841 (68.7%)	8,522	5,517 (32.0%)	2,820 (33.1%)	4.9×10^{-151}

Table 4b. Numbers and sequence coverages (%) of genes and neuron genes in hg38

1, Genes	2, Neuron genes
30077 (51.6%)	6854 (22.8%)

Table 4c. Numbers and rate of potential insertion sites for PB, SB and TcBuster in hg38

	1, Number of potential insertion sites in hg38	2, Number & % of potential insertion sites in genes in hg38	3, Number & % of potential insertion sites in neuron genes in hg38
Ifp2 (TTAA)	18,713,270	9,943,117 (53.1%)	4,521,501 (24.2%)
sleeping beauty (TA)	152,412,514	92,065,399 (60.4%)	36,803,438 (24,1%)
TcBuster (NNNTANNN)	130,938	74,733 (57.1%)	33,940 (25.9%)

*, ISCR = insertion sites-containing regions, i.e. plus 1000 bp upstream and downstream each insertion site ; **, 2 genes can overlap an ISCR; ***, each genes and neurons genes = exons and introns of their transcriptional unit plus 5000 bp upstream and downstream; ****, hypergeometric test using H0 = no enrichment in neuron genes among genes overlapped by an ISCR.

Table 5. Significant ontology terms resulting from the analysis of the 817 genes shared by PB, PB.NLS-1-558, Mm523 and Hs524.

GO ID	GO Term	P Value*	Nr. Genes
Fused GO terms: kinase activity (10.62% genes)			
GO:0016301	kinase activity	0,004222	80
Fused GO terms: establishment of cell polarity (2.26 % genes)			
GO:0030010	establishment of cell polarity	0,004364	17
Fused GO terms: cranial nerve morphogenesis (2.92% genes)			
GO:0021602	cranial nerve morphogenesis	0,000393	9
GO:0021953	central nervous system neuron differentiation	0,030239	19
Fused GO terms: regulation of signal transduction (25.76% genes)			
GO:0023051	regulation of signaling	0,008051	161
GO:0048583	regulation of response to stimulus	0,013282	183
GO:0010646	regulation of cell communication	0,005835	160
GO:0009966	regulation of signal transduction	0,001688	145
Fused GO terms: synapse organization (6,51% genes)			
GO:0034330	cell junction organization	0,001312	49
GO:0034329	cell junction assembly	0,023703	32
GO:0050808	synapse organization	0,000431	36
GO:0099173	postsynapse organization	0,005316	19
GO:0099084	postsynaptic specialization organization	0,013763	8
Fused GO terms: regulation of small GTPase mediated signal transduction (14.61% genes)			
GO:0044093	positive regulation of molecular function	0,018196	92
GO:0007264	small GTPase mediated signal transduction	0,004348	40
GO:0008047	enzyme activator activity	0,013464	37
GO:0043087	regulation of GTPase activity	0,000939	37
GO:0060589	nucleoside-triphosphatase regulator activity	0,000800	30
GO:0030695	GTPase regulator activity	0,000726	28
GO:0043547	positive regulation of GTPase activity	0,022595	30
GO:0051056	regulation of small GTPase mediated signal transduction	0,000102	31
GO:0005096	GTPase activator activity	0,000898	26
Fused GO terms:nervous system development (37.32% genes)			
GO:0007275	multicellular organism development	0,000027	238
GO:0009653	anatomical structure morphogenesis	0,000016	139
GO:0060322	head development	0,002424	53
GO:0000902	cell morphogenesis	0,000148	67
GO:0032989	cellular component morphogenesis	0,001750	52
GO:0048468	cell development	0,006713	107
GO:0048731	system development	0,000513	212
GO:0051128	regulation of cellular component organization	0,020339	114
GO:2000026	regulation of multicellular organismal development	0,048972	100
GO:0048513	animal organ development	0,035004	158
GO:0000904	cell morphogenesis involved in differentiation	0,004732	49
GO:0007399	nervous system development	0,000000	142
GO:0007417	central nervous system development	0,000026	69
GO:0022008	neurogenesis	0,000002	99
GO:0051960	regulation of nervous system development	0,001844	59
GO:0120036	plasma membrane bounded cell projection organization	0,000084	88
GO:0007420	brain development	0,005967	50
GO:0120035	regulation of plasma membrane bounded cell projection organization	0,023390	44
GO:0048699	generation of neurons	0,000001	96
GO:0120039	plasma membrane bounded cell projection morphogenesis	0,000663	48
GO:0030182	neuron differentiation	0,000000	90
GO:0048666	neuron development	0,000141	71

GO:0045664	regulation of neuron differentiation	0,047755	42
GO:0031175	neuron projection development	0,000310	64
GO:0048667	cell morphogenesis involved in neuron differentiation	0,001687	43
GO:0016358	dendrite development	0,043162	22
GO:0061564	axon development	0,013767	37
GO:0007409	axonogenesis	0,010504	35

*Term PValue corrected with Bonferroni step down. GO terms related to neurogenesis and neuron

Figure 1

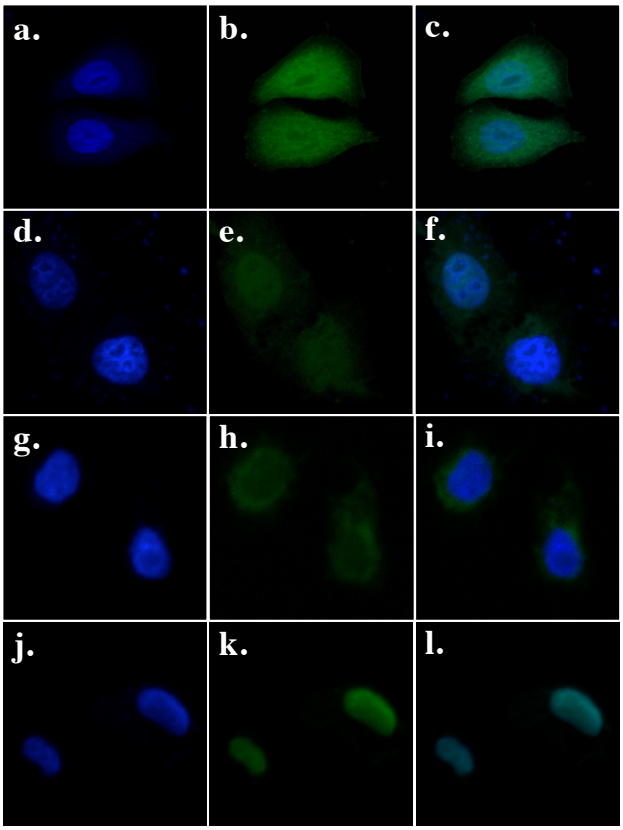

Figure 2

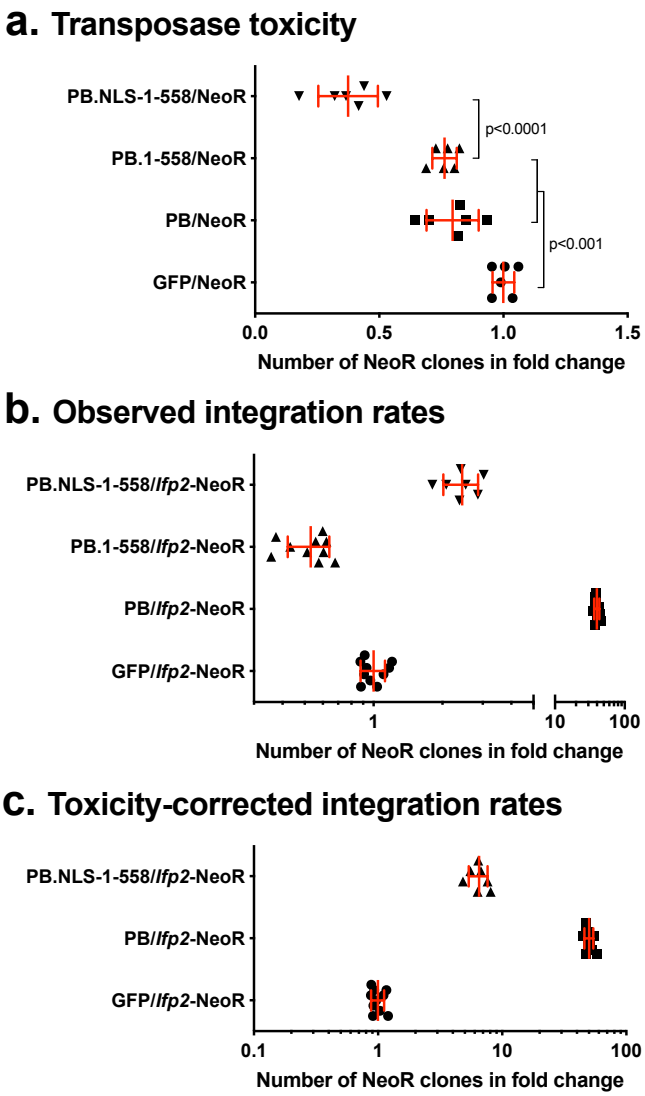
a. Transposase toxicity
PB.NLS-1-558/NeoR
PB.1-558/NeoR
PB/NeoR
GFP/NeoR
p<0.0001
p<0.001
0.0
0.5
1.0
1.5
Number of NeoR clones in fold change
b. Observed integration rates
PB.NLS-1-558/lfp2-NeoR
PB.1-558/lfp2-NeoR
PB/lfp2-NeoR
GFP/lfp2-NeoR
1
10
100
Number of NeoR clones in fold change
c. Toxicity-corrected integration rates
PB.NLS-1-558/lfp2-NeoR
PB/lfp2-NeoR
GFP/lfp2-NeoR
0.1
1
10
100
Number of NeoR clones in fold change

Figure 3

a. *lfp2*-NeoR/PB (7623 junctions)

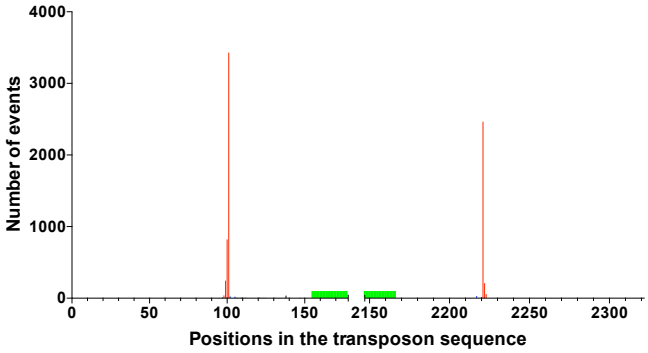

b. *lfp2*-NeoR/PB.NLS-1-558 (516 junctions)

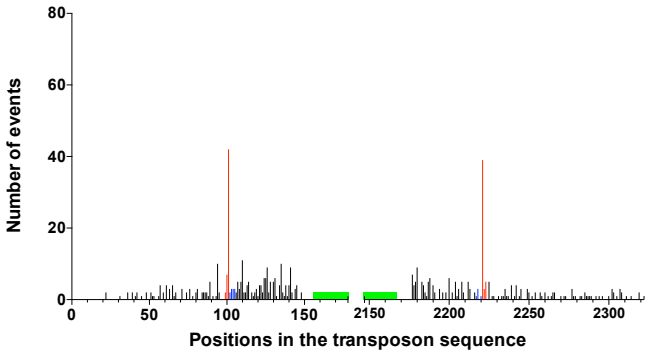

c. *lfp2*-NeoR/Mm523 PGBD5 (1461 junctions)

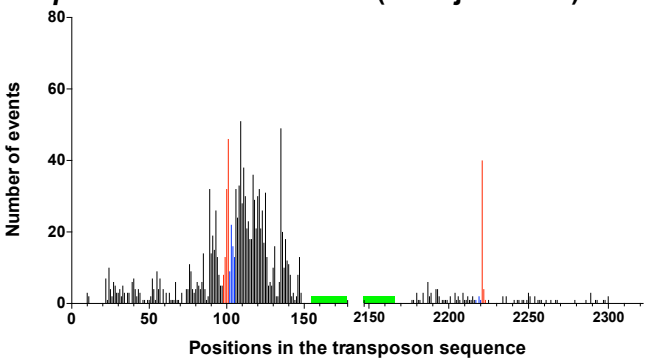

d. *lfp2*-NeoR/Hs524 PGBD5 (1051 junctions)

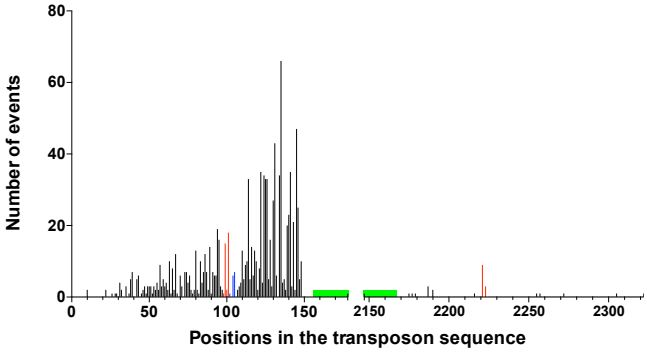

Figure 4

a.

b. PB.NLS-1-558 sequence.

MPKKKRKVKQRSAATMGSSLDDEHILSALLQSDDELVGEDSDSEISDHVSEDDVQSDTEEAFIDEVHEVQPTSSGSEILDEQNVIEQPGSSLASNRILTLPQRTIRGKNK

HCWSTSKSTRRSRVSALNIVRSQRGPTR-MCRNIYDPLLCFKLFFTDEIISEIVKWTNAEISLKRRESMTGATFRDTNEDEIYAFFGILVMTAVRKDNHMSTDDLFDRSL

SMVYVSVMSRDRFDFLIRCLRMDDKSIRPTLRENDVFTPVRKIWDLFIHQCIQNYTPGAHLTIDEQLLGFRGRCPFRMYIPNKPSKYGIKILMMCDSGTKYMINGMPYLG

RGTQTNGVPLGEYYVKELSKPVHGSCRNITCDNWFTSIPLAKNLLQEPYKLTIVGTVRSNKREIPEVLKNSRSRPVGTSMFCFDGPLTLVSYKPKPAKMVYLLSSCDEDA

SINESTGKPQMVMYYNQTKGGVDTLDQMCSVMTCSRKTNRWPMALLYGMINIACINSFIIYSHNVSSKGEKVQSRKKFMRNLYMSLTSSFMRKRLEAPTLKRYLRDNISN

ILPNEVPG

Figure 5

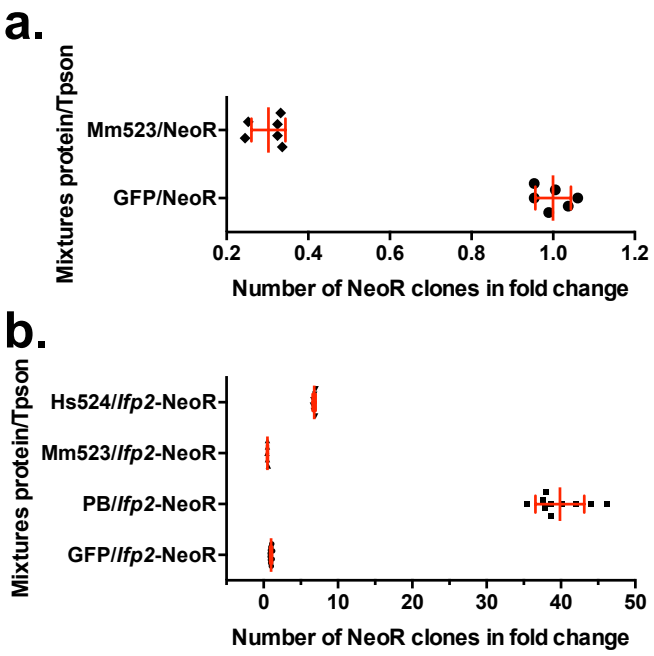
a.
Mixtures protein/Tpson
Mm523/NeoR
GFP/NeoR
0.2
0.4
0.6
0.8
1.0
1.2
Number of NeoR clones in fold change
b.
Mixtures protein/Tpson
Hs524/lfp2-NeoR
Mm523/lfp2-NeoR
PB/lfp2-NeoR
GFP/lfp2-NeoR
0
10
20
30
40
50
Number of NeoR clones in fold change

Figure 6

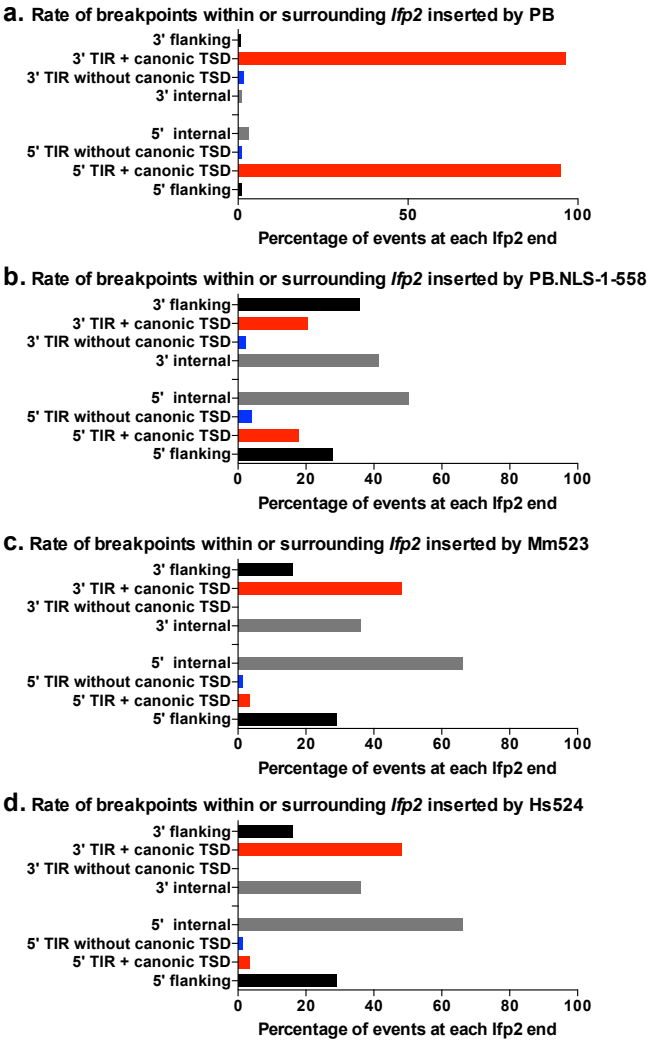
a. Rate of breakpoints within or surrounding lfp2 inserted by PB
3' flanking
3' TIR + canonic TSD
3' TIR without canonic TSD
3' internal
5' internal
5' TIR without canonic TSD
5' TIR + canonic TSD
5' flanking
0
50
100
Percentage of events at each lfp2 end
b. Rate of breakpoints within or surrounding lfp2 inserted by PB.NLS-1-558
3' flanking
3' TIR + canonic TSD
3' TIR without canonic TSD
3' internal
5' internal
5' TIR without canonic TSD
5' TIR + canonic TSD
5' flanking
0
20
40
60
80
100
Percentage of events at each lfp2 end
c. Rate of breakpoints within or surrounding lfp2 inserted by Mm523
3' flanking
3' TIR + canonic TSD
3' TIR without canonic TSD
3' internal
5' internal
5' TIR without canonic TSD
5' TIR + canonic TSD
5' flanking
0
20
40
60
80
100
Percentage of events at each lfp2 end
d. Rate of breakpoints within or surrounding lfp2 inserted by Hs524
3' flanking
3' TIR + canonic TSD
3' TIR without canonic TSD
3' internal
5' internal
5' TIR without canonic TSD
5' TIR + canonic TSD
5' flanking
0
20
40
60
80
100
Percentage of events at each lfp2 end

Figure 7

a. Occurrence of *pble* insertion sites in intragenic regions

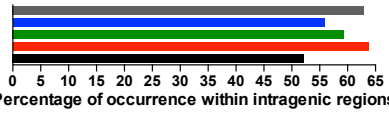

b. Occurrence of pble insertion sites around TSS (± 5 kpb)

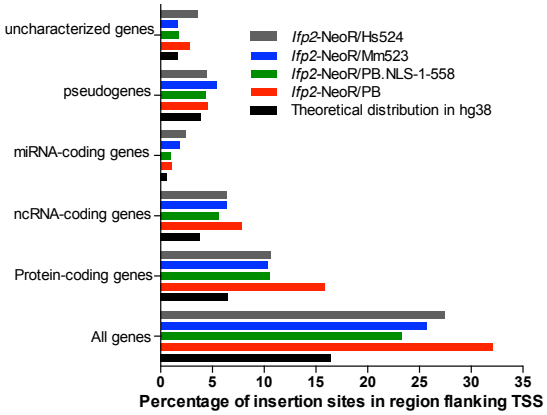

Figure 8

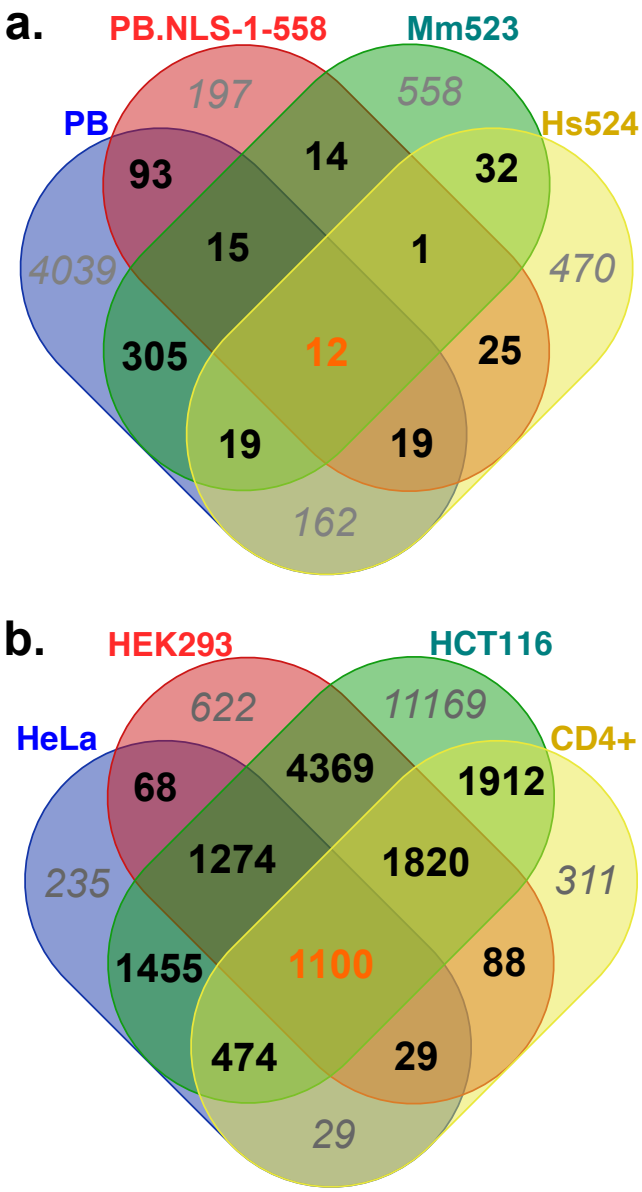
a.
PB.NLS-1-558
Mm523
PB
Hs524
197
558
4039
470
162
93
14
32
15
1
305
12
25
19
19
b.
HEK293
HCT116
HeLa
CD4+
622
11169
235
311
29
68
4369
1912
1274
1820
1455
1100
88
474
29